

Multi-Disciplinary Role of Atomic Astrophysics: From Stellar Interiors to Cancer Research Via Nanotechnology

Anil K. Pradhan^{1,2}, Sultana N. Nahar¹, Maximiliano Montenegro¹, Enam A. Chowdhury³, Kaile Li⁴, Chiranjib Sur⁵, and Yan Yu⁶

¹ Department of Astronomy, The Ohio State University, Columbus Ohio 43210, USA pradhan.1@osu.edu

² Chemical Physics Program, Department of Chemistry, The Ohio State University

³ Department of Physics, The Ohio State University

⁴ Radiation Oncology Division, The Ohio State University Medical School

⁵ High Performance Computing Group, IBM India Software Lab, Bangalore 560 071, India, chiranjib.sur@in.ibm.com

⁶ The Thomas Jefferson University Medical College, Philadelphia, PA 19107, USA yan.yu@jefferson.edu

Summary. We discuss the application of atomic physics to two diverse topics: Astrophysical opacities that determine the flow of radiation through the interior of stars, and biomedical research using nanotechnology for novel methodologies for cancer diagnostics and therapy (theranostics). Recent determination of solar abundances suggests that a re-examination of the absolute accuracy of these opacities might be in order. A discussion of the Opacity Project work and possible sources of missing opacity and uncertainties in atomic data is presented with a view to possible solution of the solar abundances problem. Another major application is shaping up in biomedicine and nanotechnology: A paradigm change and transition from conventional broadband X-ray imaging (such as in CT scanners or common X-ray sources) to precision monochromatic spectroscopy for cancer theranostics. A novel methodology — Resonant Theranostics — is proposed to exploit K_{α} resonances due to deep inner-shell transitions that trigger Auger processes in heavy elements. The methodology can be used to build laboratory monochromatic X-ray sources for imaging using K_{α} emission, as well as for therapy using K_{α} absorption by high-Z nanoparticles or radiosensitizing agents embedded in cancerous tumors. This review of recent work demonstrates the scope and power of multi-disciplinary research in general, particularly highlighting the role of atomic physics as an enabling scientific tool from astronomy to medicine.

1 Introduction

Over two decades ago two independent projects — the Opacity Project (hereafter OP [Seaton et al. 1994; Opacity 1995]) and OPAL ([Rogers & Iglesias 1992], and references therein) — were initiated to revise the then available astrophysical opacities. The efforts were launched in response to a “plea for re-examination” [Simon 1982] of the older Los Alamos opacities, that failed to account for basic observed phenomena such as the Cepheid pulsation period ratios when incorporated in stellar interior models. As is now well known, both OP and OPAL resulted in considerably higher opacities, by factors of 2-3 or higher, and did indeed solve the Cepheid and other problems. Both projects involved an enormous effort, but employed quite different physical formulations for opacities calculations, for the atomic physics methods to compute the basic atomic data and the equations-of-state (EOS). Nevertheless, the final OP and OPAL results converged for the crucial quantity of interest, the Rosseland Mean Opacity (RMO), to within 10%.

However, in recent years several lines of investigation have revealed problems in stellar astrophysics related to opacities. The foremost is the unexpectedly large discrepancy in solar surface abundances, long regarded as the ‘standard’, and accurately determined from spectroscopy. But recently derived abundances from elaborate 3-D Non-Local-Thermodynamic-Equilibrium (NLTE) convection models imply a reduction in the most abundant light metals (CNO) by an astounding 30-45% [Asplund et al. 2005]. This discrepancy and possible causes have been amply discussed in literature (an extensive discussion is given by Basu and Antia [Basu and Antia 2008]). The new reduced abundances are in serious conflict with those derived from accurate observations from helioseismology and stellar interior models.

Stellar opacity is the common feature in stellar models. More to the point, the *absolute* accuracy of opacities directly determines the uncertainties in the models. The inverse relationship between opacities and abundances is obvious (To wit: Any increase in opacities would lead to commensurately lower abundances). It is estimated that an increase between 11-21% around the base of the solar convection zone $R_{\odot}(CZ) = 0.73R_{\odot}$ ($\log T \approx 6.34$) may greatly ameliorate the situation. $R_{\odot}(CZ)$ is the boundary between the radiative and the convection zone, and is one of the tightly constrained parameters from helioseismology. Analyzing many stellar models, Basu and Antia ([Basu and Antia 2008]) note that at least an increase of 10% is required (also J. Bahcall, private communication). Thus we face the conundrum: The required increase is more than the level of agreement between OP and OPAL, but numerically not by a large amount compared to the enhancement already achieved. The logical conclusion is that higher precision is needed.

Advances in theoretical methods in the intervening two decades since the OP now enable much more accurate and consistent atomic data to be computed. A number of these developments were carried out by the group at OSU, partially under the follow-up project to the OP called the Iron Project

(Hummer et al. 1993; www.astronomy.ohio-state.edu/~pradhan). At the same time, the availability of high-performance massively parallel computational platforms also makes it possible now to undertake more accurate recalculation of opacities.

2 The Need for Re-examination of Opacities

This critical discussion entails the atomic physics of missing opacity, accuracy, and consistency of OP data. In the OP work about two decades ago we devoted considerable effort to compute atomic data using the state-of-the-art R-matrix method [Hummer et al. 1993]. A primary feature of the R-matrix method is the inclusion of radiative excitations via autoionizing resonances in photoionization cross sections. But its application to large-scale calculations necessitated compromises in accuracy, as described in the seminal paper summarising the OP work ([Seaton et al. 1994]). Some of these were: neglect of relativistic fine structure, high-energy cross sections, and inner-shell excitations.

In addition to accuracy, a bigger problem turned out to be completeness. The R-matrix calculations (even the non-relativistic version employed in the OP) became too cumbersome for the codes and computational resources available at that time. Therefore, a considerable amount of radiative data was computed with a much simpler method, using the atomic structure code called SUPERSTRUCTURE. For example, most of the data for iron ions Fe VIII–XIII was thus obtained (referred to as the PLUS data in [Seaton et al. 1994]). Based on OPAL work, it was known that these Fe ions are of crucial importance around the so-called Z-bump, vital for Cepheid pulsation models around $\text{Log}(T) \approx 5.2\text{--}5.3$. That is because there are a huge number of M-shell transitions $n = 3 \rightarrow n' \geq 3$: The problem with the inner-shell data was also redressed in the past few years using another version of SUPERSTRUCTURE [Seaton & Badnell 2004].

Could there still be some atomic data that might result in missing opacity? In spite of the inclusion of inner-shell data, the outer-shell atomic data in the revised OP calculations remained the same Seaton et al. 1994. Therefore, a number of resonance complexes corresponding to several Rydberg series of levels were not included. Many calculations since the OP work, particularly under the Iron Project by the OSU group, have shown that outer-shell radiative excitations into autoionizing resonances that lie *below* the inner-shell ionization energies are excluded. Fig. 1 compares photoionization cross sections of an excited state of two ions in the Boron isoelectronic sequence, O III and Fe XXI, from OP and from more recent work. The cross sections exhibit huge *photoexcitation-of-core* (PEC) resonances (first identified by Yu and Seaton [Seaton et al. 1994]). These complexes of (PEC) resonances converge on to the inner-shell ionization threshold energy with a large jump. But the crucial fact is that the effective cross sections are much higher than the

OP data, and enhanced throughout the $n = 2 - 3$ energy range by up to two orders of magnitude.

As inferred from Fig. 1, the missing opacity may lie in an energy range from few eV to few hundreds of eV, depending on the element and ionization stage. Low-lying excited states of most ionization stages of abundant elements exhibit similar structures. This could be of direct relevance at temperatures and densities up to $R_{\odot}(CZ)$ around $\text{Log } T \sim 6$.

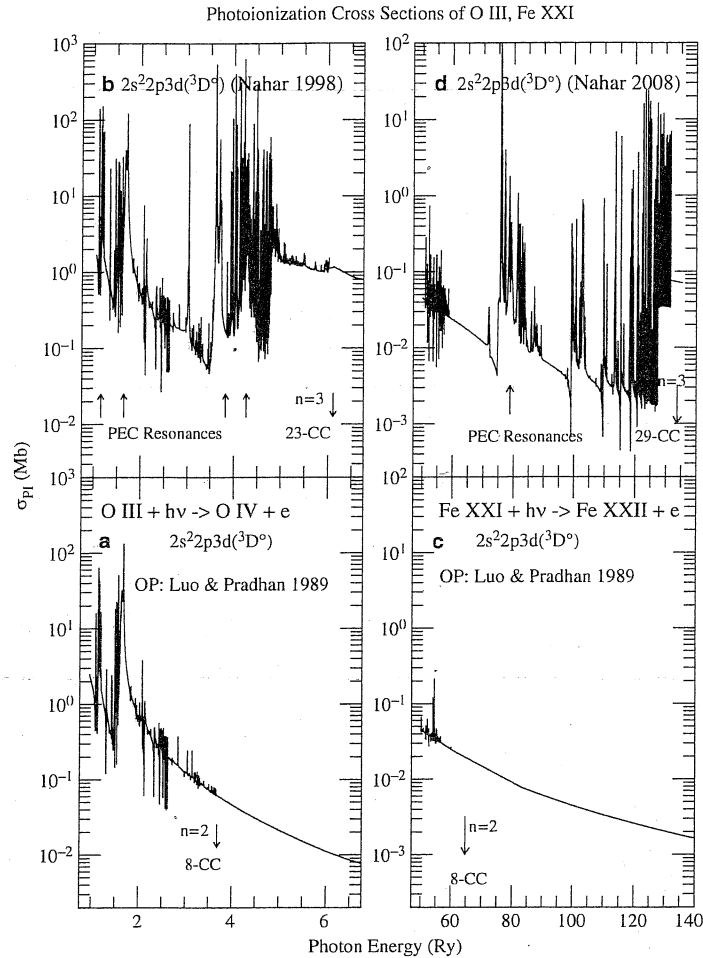


Fig. 1. Missing resonances in photoionization cross sections of C-like O and Fe: bottom panels (a,c) — OP data, top panels (b,d) — more recent calculations which show that large resonance complexes were not included in OP data, and could account for some missing opacity. Note the abscissa in Rydbergs. References: Nahar 1998 [Nahar 1998], Luo and Pradhan [Seaton et al. 1994].

Apart from limited treatment of atomic structure, affecting accuracy and resulting in missing resonances, the OP atomic calculations were non-relativistic and in LS coupling. Therefore, a significant omission is that of intercombination transitions that involve spin-change but are permitted by change in parity and angular momentum. Although the total line strength in intercombination lines is only a fraction of that in dipole allowed transitions

(no spin-change), both are E1 transitions and the effect is of the order of 15–20%. A limited number of intercombination lines ($n \leq 6$) were included later [Seaton & Badnell 2004]. But, as mentioned above, since most of the OP data for Fe ions does *not* employ the R-matrix method, we expect the *absolute accuracy* to be no better than the OPAL data also computed using an atomic structure code (with a parametrized atomic potential). Therefore it would not be surprising if it is ascertained that there are systematic uncertainties in both the OP and OPAL data.

Although much of fine structure splitting is subsumed by line broadening, a proper treatment should incorporate relativistic fine structure more accurately than the current OP data. In the past few years, members of the OSU group, especially former graduate student G.X. Chen in collaboration with W. Eissner, have developed an extended version of the relativistic R-matrix method in the Breit-Pauli approximation used in the Iron Project work [Hummer et al. 1993]. The OP data were computed or obtained in a variety of approximations and sources. In particular, the iron data was from six different sources, which raises some concern about consistency if not accuracy. And it was known that the loss of accuracy owing to restricted approximations for the low-ionization stages of iron Fe I–V, and other Fe-group elements, was especially severe [Seaton et al. 1994; Seaton & Badnell 2004]. It therefore became necessary to include the corresponding transition probabilities from other sources. Although low ionization stages do not affect the RMOs in a significant manner, they are crucial in computing radiative accelerations, and may well account for some of the large differences between OP and OPAL [Delahaye & Pinsonneault 2006].

3 Opacity and Radiation Force

Once the opacity is known, the radiative force exerted by photons on a given atom may be readily computed, and photon absorption and scattering processes are responsible for radiation pressure. Opacities and radiative accelerations computed by OP have been made available from an electronic dataserver called OPSERVER (Mendoza et al. [Mendoza et al. 2007]), located at the Ohio Supercomputer Center at OSU and accessible from: <http://opacities.osc.edu>. Fig. 2 is a schematic diagram for the computation of OP opacities.

It is a non-trivial task to process all of the archived atomic data for proper input into the opacities code. It involves interface and mapping of data at computing energies onto a photon-frequency mesh. The standard variable for mapping is $u = h\nu/kT$. We define a “Rosseland window” in the range $-2.5 \leq \text{Log } u \leq 1.5$, which samples the monochromatic opacity with a given number of mesh points. Given the frequency-temperature correlation from the EOS, and the Planck function, the u -range is chosen so as to ensure that there is negligible contribution to opacity for any ion from outside the Rosseland window. This task is performed by the code INTERFACE (Pradhan,

RADIATIVE OPACITIES AND ACCELERATIONS

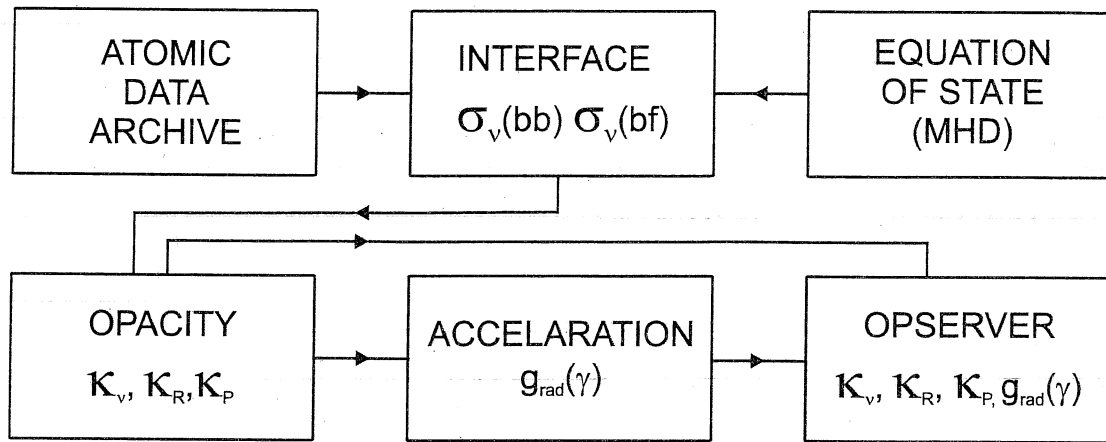


Fig. 2. Schematic diagram of OP opacities computations.

unpublished), which also computes radiative line damping parameters using the bound-bound radiative transition probabilities, labeled as 'bb-data' which contains f -values for all allowed and intercombination E1 transitions. INTERFACE maps and produces the bb files as well as the files for bound-free photoionization cross sections, labeled as bf files, for each ion.

The MHD EOS code [Seaton et al. 1994] independently produces tables of ionization fractions, scattering contributions, Stark broadening, and other parameters. The first calculation would be to use the standard EOS data as in the current OP. Later steps would follow as mentioned above.

The opacities code OPACITY requires the bb and bf atomic data files from INTERFACE and the EOS tables. Calculations for the monochromatic opacity κ_ν are carried out for each ion along isotherms in $\text{Log } T$ for a range of Log electron densities N_e . It is also useful to tabulate results along the variable $R = \rho/T_6^3$ ($T_6 = T \times 10^{-6}$) defined by OPAL. The Rosseland Mean Opacity κ_R is defined in terms of κ_ν as

$$\frac{1}{\kappa_R} = \frac{\int_0^\infty g(u) \frac{1}{\kappa_\nu} du}{\int_0^\infty g(u) du}, \quad g(u) = u^4 e^{-u} (1 - e^{-u})^{-2}, \quad (1)$$

where $g(u)$ is the Planck weighting function corrected for stimulated emission. The κ_ν is primarily a function of the oscillator strengths f , photoionization cross sections σ_ν , level populations N_i , and the line profile factor ϕ_ν ,

$$\kappa_\nu^{bb}(i \rightarrow j) = \left(\frac{\pi e^2}{m_e c} \right) N_i f_{ij} \phi_\nu, \quad \kappa_\nu^{bf} = N_i \sigma_\nu. \quad (2)$$

Fig. 3 illustrates $\kappa_\nu(\text{Fe IV})$ recently computed using the more accurate and extensive radiative R-matrix calculations by Nahar and Pradhan [Nahar & Pradhan 2005] including fine structure, compared to the original OP data. The difference in the Rosseland means is up to 50% at the (T, N_e) shown (close to maximum abundance of Fe IV). Although the Nahar and Pradhan calculations were also in LS coupling, they used a much larger wavefunction expansion than in the OP work. As noted, for such reasons the final OP calculations used the more complete bb data for lines of Fe I–V from the Kurucz database (R.L. Kurucz: www.harvard.edu/amp, which also includes fine structure). Fig. 3 shows the importance of completeness, but the accuracy issue is unresolved.

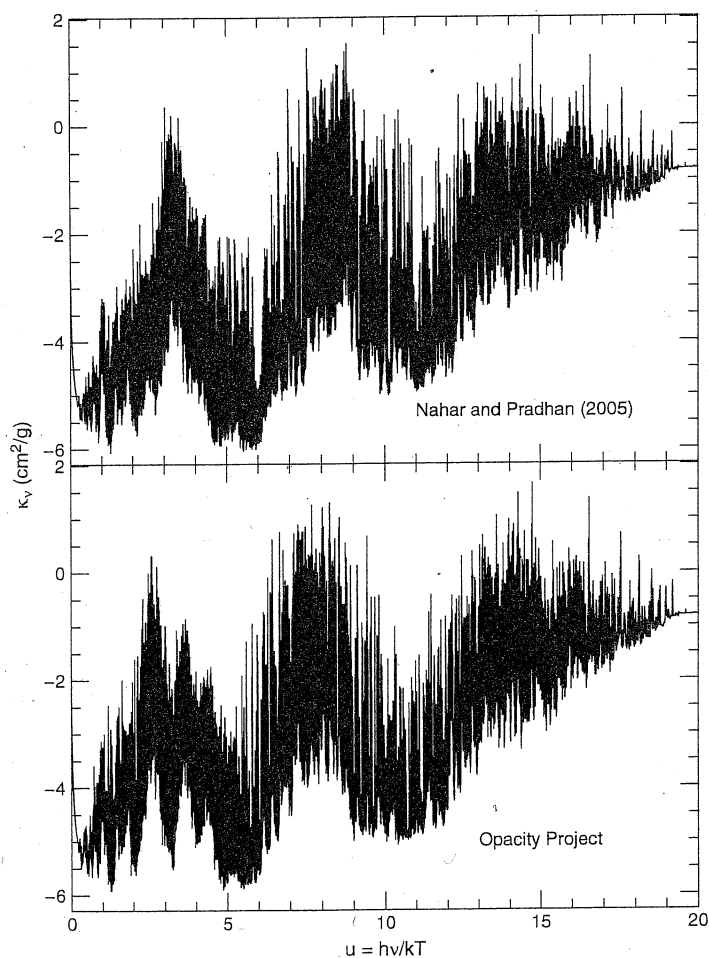


Fig. 3. Monochromatic opacity of Fe IV at $\text{Log } T(\text{K}) = 4.5$ and $\text{Log } N_e(\text{cm}^{-3}) = 17$ — Recent calculations using new R-matrix calculations with fine structure (Nahar and Pradhan [Nahar & Pradhan 2005]), and the original OP data [Seaton et al. 1994]. Although the overall features look similar, there are considerable differences in detail and in Rosseland Mean Opacities of 10-50%.

4 SUMMARY: The Opacity Project and the Solar Abundance Problem

The possible solution to fundamental problems with solar models that have emerged in recent years appears to lie in stellar opacity. Helioseismology, equations-of-state, solar abundances, and stellar interiors models, are discordant in surprising and unexpected manner. The practical necessity of solving this problem can hardly be overstated, owing to the Sun as the standard that is the key to understanding much of astrophysics. As noted by stellar researchers, a 10-20% revision of opacities would go a long way to resolving many discrepancies. At the same time, the minimum uncertainties in atomic physics are at least in that range if not much higher. In addition, computed theoretical data reveal several sources of missing opacity or *systematic* inaccuracy in the approximations employed.

5 From Stellar Opacities to Resonant Theranostics

In summary, there is some uncertainty in existing opacities calculations owing to the fact that resonances due to inner-shell excitations have not yet been fully included. Related effects such as autoionization widths, and plasma broadening, are not accounted for. However, the *resonance phenomena* so extensively studied under the OP have found a novel, and surprising, application in biomedical physics aimed at cancer diagnostics and therapy (theranostics) using nanotechnology.

6 Resonant Theranostics

Recently, we have proposed an integrated scheme for X-ray Resonant Theranostics (therapy and diagnostics) along these lines [Silver et al. 2008; Pradhan et al. 2009; Montenegro et al. 2009] based on resonant monochromatic X-ray sources. X-rays interact efficiently with high-Z elements and many radiosensitized reactive agents are molecular compounds or moieties containing heavy elements, such as bromodeoxyuridine (BUdR), iododeoxyuridine (IUdR) and cisplatin (cis-Pt) with bromine, iodine, and platinum ($Z = 35, 53, \text{ and } 78$) respectively. BUdR and IUdR are widely used in medical imaging, cisPt or Cyclo-Pt are utilized in cancer therapy. The high-Z elements undergo Auger fluorescence when irradiated by X-rays at energies, for example, above the ionization energy of the innermost (K) shell. Radiation induced ionization of atoms can cause DNA strand breakups in malignant cells. Low-energy electrons resulting from Auger breakups can cause single and double strand DNA breakups via electron attachment resonances (references in [Pradhan et al. 2009]).

However, while X-ray interaction with heavy elements is well known, the detailed physical properties of high-Z elements are relatively unknown, either

experimentally or theoretically. The problem becomes progressively more difficult with Z , especially for elements at the high-end of the periodic table such as gold, which is finding increasing usage in nanobiotechnology. Gold is generally non-reactive and therefore ideal for constructing nanoparticles for medical use for *in vivo* treatment. Laboratory experiments using gold nanoparticles injected into mice tumors, and then irradiated with high energy 140-250 keVp X-rays, have shown considerable reduction in tumor sizes [Hainfield et al. 2004; Cho 2005]. Gold is particularly appropriate for such experiments owing to its non-toxicity and high Z ($= 79$). Nanoparticle form entails sizes from a few to a few tens of nm, and in principle sufficient to penetrate cell vascula provided the size is < 30 nm or so. X-ray irradiation then enhances the radiation dose uptake, with consequent damage to the malignant cells with embedded nanoparticles.

6.1 Broadband vs. Monochromatic X-rays Sources

The broadband radiation sources employed in these experiments are the generally available X-ray generators in medical facilities. They are X-ray sources with energy output in the form of a bremsstrahlung spectrum, and deliver radiation up to the stated peak voltage. The shape of the output bremsstrahlung spectrum extends up to the peak voltage (kVp) between the cathode and the anode of the generating X-ray tube. Most of the flux from traditional X-ray sources covers an extremely broad range, well over half the total energy range, and a maximum around $1/3$ the peak value [Sundaraman et al. 1973]. For example, for a 250 kVp source the X-ray output ranges between 40-250 keV photon energies, with a broad maximum around ~ 80 keV. Since the Au K-edge $E_I(K) = 80.729$ keV, a 250 kVp source is capable of ionizing all inner n -shells and subshells of the gold atom with L,M,N,O,P edges at approximately 12-14, 3.4-2.2, 0.11-0.9, 0.01-0.11, 0.0009 keV respectively. Of course, much higher energy accelerators are also in common medical usage, say those with up to 6 MVp peak voltage and a broad maximum around 2 MeV.

The main problem with using broadband bremsstrahlung X-ray sources (ordinary devices, accelerators, or CT scanners) is as follows. The low-energy (~ 10 -30 keV) flux is absorbed by body tissue close to the skin before reaching the desired target (e.g. tumor); at the same time high-energy X-rays (> 1 MeV) barely interact with the light elements and compounds (e.g. H_2O). Therefore, both the low-energy and the high-energy X-rays are inefficient in terms of proper medical use in imaging or therapy. For optimal usage and to obviate unnecessary exposure to healthy tissue the incident X-rays should be in precisely the right energy range, which can be pre-determined, commensurate with dosimetric parameters such as depth and shape as well as the particular physical chemistry of the radiosensitizing agents. But relatively high energy X-rays still are needed to ensure sufficient penetration and to minimize photoabsorption which scales roughly as E^{-3} [NIST]. With the exception of the K-edges, the photoionization cross section decreases rapidly

with energy and the efficiency of radiation absorption diminishes. Therefore, the incident X-rays need to be not only monochromatic but also pre-selected for maximum interaction cross sections. While it is promising that irradiation and subsequent breakup of high-Z atoms may be a useful tool in cancer theranostics, the precise interaction of X-rays as a function of incident energy and the target atomic structure needs to be studied in order to understand and improve the techniques and the concepts involved. The primary aim of this review is to outline, in principle, the theranostical efficacy of monochromatic X-rays with high-Z elements.

But while broadband X-ray sources are generally used in medical practice, narrow-band or monochromatic X-ray sources such as synchrotron based devices and laser produced plasmas are available [Zhavoronkov et al. 2005; Andiel et al. 2001; Moribayashi et al. 2001; Berger & Motz 2004]. The most useful characteristic of these sources is their capability to generate monochromatic beams of high intensity photon fluxes. Indeed it is well known that the output spectra of ordinary X-ray tubes prominently display $K\alpha$, $K\beta$ emission lines superimposed on a bremsstrahlung background [Sundaraman et al. 1973], and can be easily isolated, albeit with lower X-ray fluxes which may still be used for diagnostic imaging. Devices widely employed in X-ray atomic physics such as the Electron-Beam-Ion-Traps may be used as possible monochromatic sources [Silver et al. 2008]. In addition, advances are being made in generating ultrashort K-shell radiation using femtosecond laser pulses impinging on thin solid material [Reich et al. 2000]. These sources can be utilized not only for basic studies of matter at atomic and molecular scales, but also to probe materials at nanoscales for applications to nanotechnology and biomedical imaging and spectroscopy. Large energy deposition in a small target would produce a transient plasma on short time scales. It is of interest to investigate the material properties of such 'plasmoids', and to ascertain the related physical constants as a function of the incident X-ray energy and nuclear charge Z all along the Periodic Table, and other extrinsic parameters such as density and size of the targeted material.

6.2 Auger Processes: Monochromatic X-ray Diagnostics and Therapeutics

The relevant atomic and molecular computations are extremely difficult owing to the fact that both the relativistic effects and many-electron correlation effects need to be considered explicitly. Moreover, careful attention needs to be paid to the energy dependence on the incident photon energy, particularly in energy ranges where resonant phenomena occur with large transition probabilities and cross sections. Available cross sections for attenuation of X-rays by the atoms of different elements have been computed using atomic physics methods that yield only the background cross sections, as from the on-line databases at the *National Institute for Standards and Technology* (NIST: www.nist.gov [NIST]). For molecular systems containing a given

high-Z element, we assume that the dominant X-ray interaction is with that element.

Fig. 4 shows these photoelectric attenuation coefficients for high-Z neutral Fe and Au, compared with a low-Z element O.

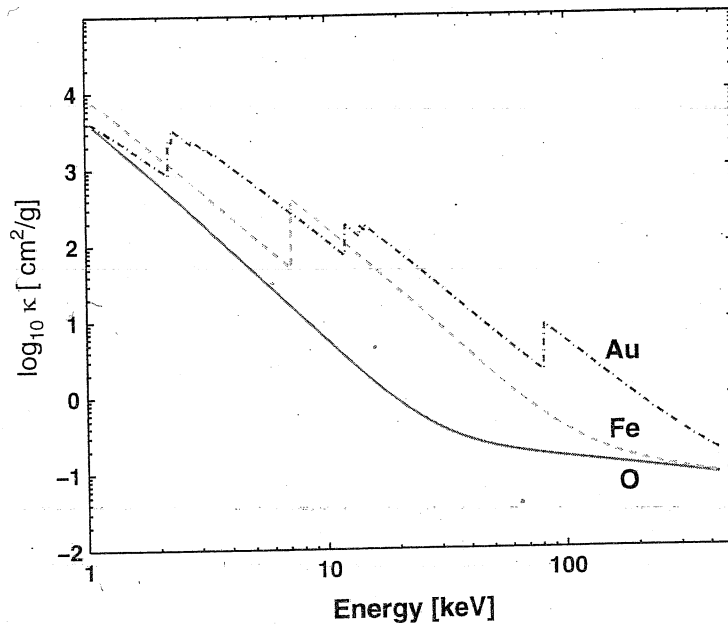


Fig. 4. Background photoabsorption attenuation coefficients κ NIST for neutral O, Fe, and Au. The rise in κ at various energies correspond to ionization edges of the K, L, M (sub)-shells of Au, and the K-shell of Fe. The oxygen K-edge lies at 0.53 keV and is not seen (from [Pradhan et al. 2009]).

K-shell ionization may be initiated by any photon with energy above the K-edge. As shown in Fig. 5, that would trigger Auger decays leading to a cascade of secondary photon emission and electron ejection. The most probable decay is K_{α} emission, that occurs with fluorescence yield of over 95% in the $L \rightarrow K$ transition in high-Z atoms [Pradhan et al. 2009].

6.3 Monochromatic X-ray Emission for Imaging

Using a broadband X-ray source, such as readily available in medical facilities and which produce a bremsstrahlung output spectrum from an ordinary X-ray tube, we can generate pure monochromatic K_{α} radiation. Perhaps the earliest example to scatter broadband radiation and isolate a monochromatic wavelength was in 1923 when Arthur Compton demonstrated the Compton effect in [Compton 1923a,b]. He used a Molybdenum anode X-ray tube to reflect X-rays from a graphite plate at different angles: 45, 90, and 135 degrees. That produced monochromatic Mo K_{α} X-rays which were then scattered from a crystal to measure the wavelength shift precisely using the Bragg formula. However, Compton noted that while eliminating the bremsstrahlung background, the intensity of Mo K_{α} radiation was reduced by a factor of 1/25000.

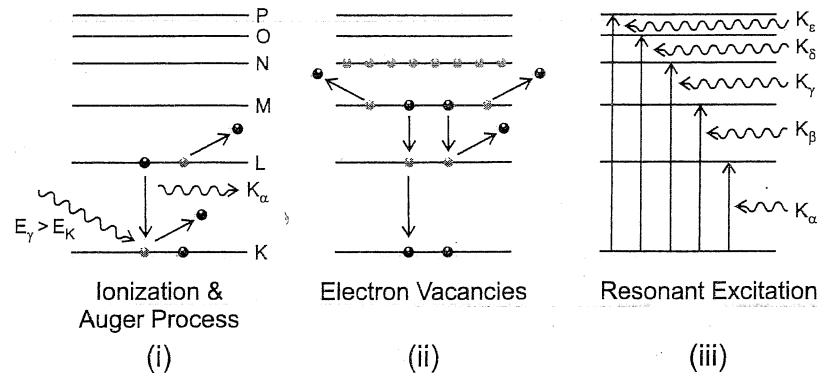


Fig. 5. The Auger process and resonant excitation (from [Pradhan et al. 2009]): (i) K-shell ionization, $K\alpha$ emission and/or L-shell Auger electron emission, (ii) multiple electron vacancies created by K-shell ionization due to Auger electron ejections from higher shells and radiative decays, (iii) resonant excitation from the K-shell to higher shells by $K\alpha$, $K\beta$, etc. by incident photons. The gold atom has electronic shells up to $n = 6$, or the P-shell.

A gas cell or solid target of high- Z material may be irradiated by an X-ray tube that produces broadband bremsstrahlung radiation. The $K\alpha$ radiation would be emitted isotropically and may be detected perpendicular to the primary X-ray beam at 90 degrees, as in the classic Compton configuration or adaptation thereof. X-ray imaging can then be carried out using monochromatic $K\alpha$ emission, with little background (as noted by Compton in 1923!) and vastly reduced radiation exposure compared to the broadband X-ray source itself. Since the $K\alpha$ emission is isotropic, it is reduced by a geometric factor of $1/4\pi$ in any given direction. A cylindrical configuration to ameliorate this problem is proposed by Huang et al. [Huang et al.], who also carry out Monte Carlo simulations using the code GEANT4 (see also Montenegro et al. [Montenegro et al. 2009]).

6.4 Monochromatic X-ray Absorption for Therapeutics

For resonance driven therapeutics we can utilize any $K\alpha$ source of sufficient intensity for resonant absorption following K-shell ionization. Since each K-shell ionization produces one or two L-shell vacancies [Pradhan et al. 2009], resonant $K\alpha$ absorption can be achieved. For example, we may use an ordinary X-ray tube that produces bremsstrahlung radiation up to 100 keV. If the target is gold ($Z = 79$) with K-edge at ~ 81 keV, then it can produce $K\alpha$ radiation at ~ 68 keV for imaging of a target made of another element, or a combination of elements such as in body tissue. The therapeutics mechanism is complementary to imaging. We can resonantly excite gold atoms from the K-shell thereby reversing or enhancing the efficacy of Auger cascades. Resonant therapeutics can be utilized for optimally localized energy deposition at energies corresponding to Au $K\alpha$ emission/absorption at 68 keV, as well as

higher resonances due to excitation from the K-shell, as shown in Fig. 5 (iii) and via resonances in Fig. 6.

Using the transition probabilities for excitation from the K-shell into L,M,N,O and P shells of gold ions, calculated by Nahar et al. [Nahar et al. 2008]; we compute resonant attenuation coefficients shown in Fig. 6 from Pradhan et al. [Pradhan et al. 2009]. The resonant excitation cross sections in Fig. 6 can be orders of magnitude higher than the background cross sections for Au in Fig. 4.

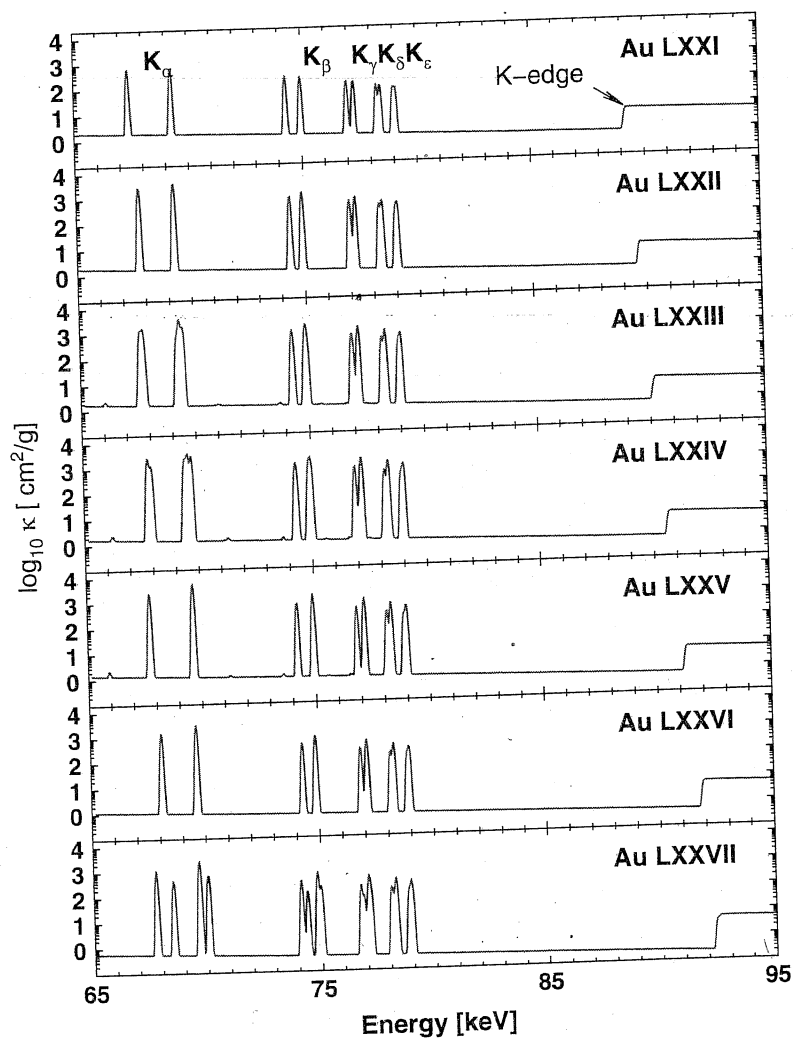


Fig. 6. Total resonant K-shell and non-resonant X-ray mass attenuation coefficients $\kappa(\text{cm}^2/\text{g})$ for gold ions (note the log scale on the Y-axis). The resonances correspond to excitation probabilities for K_α , K_β , etc. transitions in gold ions with F-like (top panel) to Li-like (bottom panel) ion cores. Resonant cross sections can be orders of magnitude higher than the K-edge jump on the extreme right.

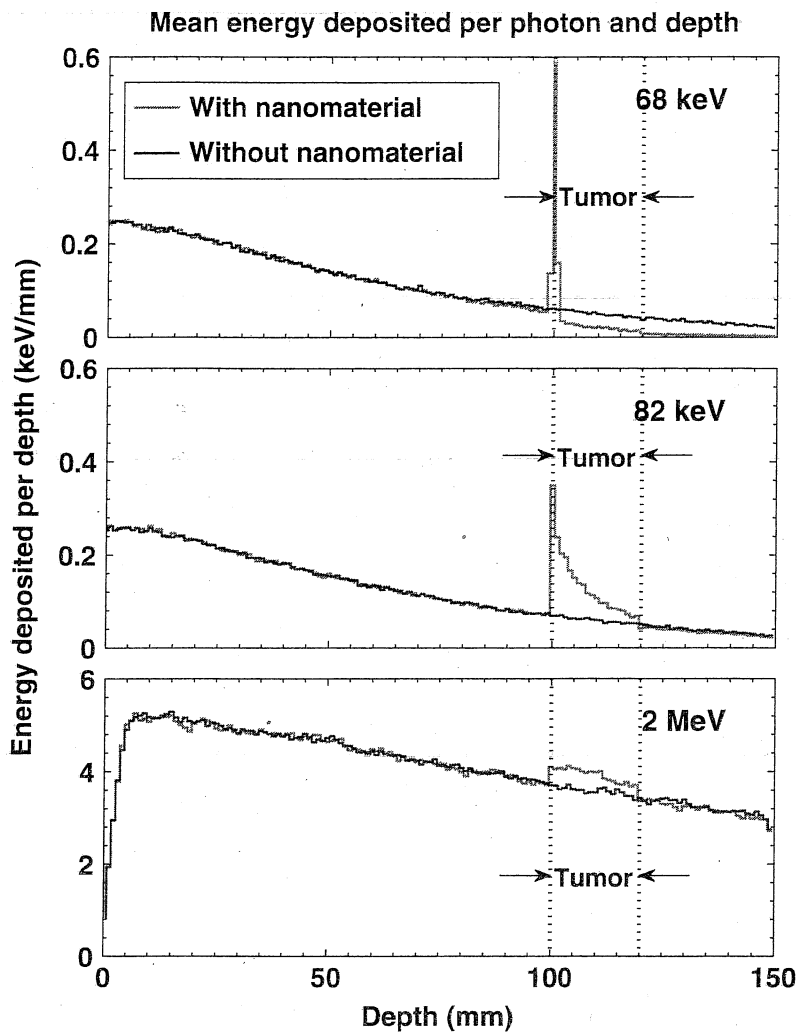


Fig. 7. Energy deposited by depth across a water phantom with a 2 cm tumor, injected with gold nanoparticles, at a depth of 10 cm in the body. Resonant energy absorption is shown for three monochromatic X-ray beams: top panel — 68 keV (averaged K_{α} resonant energy); middle panel — 82 keV (K-edge energy), and bottom panel — 2 MeV (high energy). The region between 100 and 120 mm represents the tumor embedded with gold nanoparticles at concentration of 5 mg/ml. The presence of gold nanoparticles increases the energy deposited at the tumor site; this effect is strongest at the resonant K_{α} energy (top panel) and least at the highest energy 2 MeV. The K-edge energy at ~ 82 keV has significant absorption, but much less than at 68 keV by several factors.

6.5 Monte Carlo Simulations of Resonant Absorption by Gold Nanoparticles

Montenegro et al. [Montenegro et al. 2009] have carried out numerical simulations using the Monte Carlo code GEANT4. They model a phantom that simulates a tumor located 10 cms inside the body and embedded with gold nanoparticles. Three irradiating monochromatic X-ray sources are considered: (i) the resonant K_{α} energy 68 keV, (ii) just above the K-shell ionization energy, 82 keV, where the K-shell photoionization cross section is at its maximum

(Fig. 4), and (iii) a very high energy of 2 MeV characteristic of the energy where the bremsstrahlung X-ray spectrum from linear accelerators has a broad peak. High energy linear accelerators are used as broadband X-ray sources for deeper penetration in the body for imaging and therapy. The three sets of results from GEANT4 simulations are illustrated in Fig. 7. It is seen that resonant K_{α} absorption at 68 keV can lead to a sharp peak indicating that complete absorption takes place at that energy, in contrast to less efficient absorption following the K-edge at 82 keV.

7 Conclusion

We have attempted to highlight the diversity and the range of multi-disciplinary applications of atomic physics by focusing on two major scientific problems, one in astronomy and the other in biomedicine.

We would like to acknowledge support from the Large Interdisciplinary Grants award from OSU for Computational Nanoscience on Fundamental Atomic and Molecular Scales. The computational work was carried out at the Ohio Supercomputer Center in Columbus Ohio.

Disclaimer: The material presented is that of the author (CS) and IBM is not responsible or liable for any information presented in this paper.

References

- Andiel U., Eidmann K., and Witte K., *Phys. Rev. E* 63, 026407 (2001).
 Asplund M., Grevesse N., Sauval A. J., *Cosmic Abundances as Records of Stellar Evolution and Nucleosynthesis: In ASP Conf. Ser., Vol. 336, 25, (2005).*
 Basu S. and Antia H. N., *Physics Reports*, 457, 217 (2008).
 Berger M. and Motz J. W., *Nucl. Inst. and Meth. in Phys. Res. B* 226, 327 (2004).
 Cho S. H., *Phys. Med. Biol.* 50, N163 (2005).
 Compton A. H., *Physical Review*, 21, 494 (1923a).
 Compton A. H., *Physical Review*, 22, 409 (1923b).
 Delahaye F. and Pinsonneault M., *Astrophys. J.*, 649, 529 (2006).
 Hainfield J. F., Slatkin D. N., and Smilowitz H. M., *Phys. Med. Biol.* 49, N309 (2004).
 Huang K., Pradhan A. K., Nahar S. N., Montenegro M., Yu Y., 31st Annual International IEEE EMBS Conference (in press).
 Hummer D. G., Berrington K. A., Eissner W., Pradhan A. K., Saraph H. E., and Tully J. A., *Astron. Astrophys.* 279, 298 (1993).
 Mendoza C., Seaton M. J., Buerger P., Bellorin A., Melendez M., Gonzalez J., Rodriguez L. S., Palacios E., Pradhan, C.J. Zeippen, *Mon. Not. R. astr. Soc.*, 378, 1031 (2007).
 Montenegro M., Nahar S. N., Pradhan A. K., Huang K., Yu Y., *J. Phys. Chem. A* 113, 12364 (2009).
 Moribayashi K., Sasaki A., and Zhidkov A., *Phys. Scr.* T92, 185 (2001).
 Nahar S. N., *Physical Review A* 58, 3766 (1998).

- Nahar S. N. and Pradhan A. K., *Astron. Astrophys.*, 437, 345 (2005). **2008**, 21, 30.
- Nahar S. N., Sur C., and Pradhan, A. K., *JQSRT*, 109, 1951 (2008).
- National Institute for Standards and Tchnology, Physical Reference Data (www.nist.gov/Phys.Ref.Data).
- The Opacity Project Team, *The Opacity Project* Vols. 1 & 2, Institute of Physics Publishing (1995).
- Pradhan A. K., Nahar S. N., Montenegro M., Yu Y., Zhang H. L., Sur C., Mrozik M., Pitzer R. M., *J. Phys. Chem. A* 113, 12356 (2009).
- Reich C., Gibbon P., Uschmann I., and Förster E., *Physical Review Letters* 84, 4846 (2000).
- Rogers F. J. and Iglesias C. A., *Astrophys. J. Supp. Ser.*, 79, 507 (1992).
- Seaton M. J. and Badnell N. R., *Mon. Not. R. astr. Soc.*, 354, 457 (2004).
- Seaton M. J., Yu Y., Mihalas D., and Pradhan A. K., *Mon. Not. R. astr. Soc.* 266, 805 (1994).
- Silver E., Pradhan A. K., and Yu Y., *RT Image*, 21, 30 (2008).
- Simon N. R., *Astrophys. J.*, 260, L87 (1982).
- Sundararaman V., Prasad M. A., and Vora R. B., *Phys. Med. Biol.* 18, 208 (1973).
- Zhavoronkov N., Gritsai Y., Bargheer M., Woerner M., and Elsaesser T., *Appl. Phys. Letts.* 86, 244107 (2005).